Available online at www.sciencedirect.com
SCIENCE DIRECT®
International Journal of Heat and Mass Transfer 48 (2005) 4428–4434
International Journal of HEAT and MASS TRANSFER
www.elsevier.com/locate/ijhmt

Advances in control of frost on evaporator coils with an applied electric field

V. Tudor [a,*], M. Ohadi [b], M.A. Salehi [c], J.V. Lawler [c]

[a] *Advanced Thermal Research Laboratory, Mechanical Engineering Department, US Naval Academy, Annapolis, MD 21402, USA*
[b] *Smart and Small Thermal Systems Laboratory, Mechanical Engineering Department, University of Maryland, College park, MD 20742, USA*
[c] *ATEC Inc., College Park, MD 20742, USA*

Received 10 March 2005; received in revised form 12 May 2005
Available online 14 July 2005

Abstract

This paper introduces an innovative technique on use of an applied electric field for control of frost over evaporator coils with fin density and geometric configuration of interest to freezer/refrigerator applications. The technique discussed in this paper, referred to as the "dielectric barrier discharge" (DBD) method, may be particularly suitable for application in evaporator coils with high fin density. Experiments conducted with a small-scale laboratory test-module, as well as a full-scale supermarket evaporator are presented. The DBD technique is based on generating localized non-resistive heating within fins of an evaporator coil via application of a high-voltage, alternating current through electrodes. Our experiments demonstrate that the defrosting time using DBD is substantially shorter than conventional techniques, while the energy consumption associated with the process is less than one half of the corresponding energy of the electrical resistance heating methods. Basic operational principles of the technique, its advantages and limitations when compared to conventional electrical defrosting techniques are discussed and presented for the first time in this paper.

Keywords: DBD frost melting, Refrigeration; Coil; AC current, Micro-discharge

1. Introduction

When humid air comes into contact with a surface whose temperature is below both the air dew point temperature and 0 °C (at 1 atm.) frost growth will be initiated. Frost formation and growth patterns will vary depending on the surface and air temperatures, airflow, and the humidity content in the air. Frost formation is a complex transient process in which both heat and mass transfer occur simultaneously. Frost accumulation is undesirable in tube-fin type refrigeration equipment because it results in increased heat transfer resistance as well as increased pressure drop in the system. Moreover, the frost formed on the coils or fins of heat exchangers blocks the airflow passage, leading to reduced COP and system capacity. Frequent defrosting reduces the COP of air-cooled refrigeration systems due to the

* Corresponding author. Tel.: +1 410 293 6530; fax: +1 410 293 3041.
E-mail address: vtudor@usna.edu (V. Tudor).

0017-9310/$ - see front matter © 2005 Elsevier Ltd. All rights reserved.
doi:10.1016/j.ijheatmasstransfer.2005.05.011

Nomenclature

d_d	dielectric thickness	I	current (A)
d_g	air gap thickness	t, T	time (s)
D_i	bare/inner wire diameter (mm)	V	electrical potential/voltage (V)
D_o	insulation/outer wire diameter (mm)		
DBD	dielectric barrier discharge	*Greek symbols*	
E_d	electric field strength in the dielectric (V/m)	ρ	surface charge density (C/m^2)
E_g	electric field strength in the fin gap (V/m)	ε	dielectric constant
f	frequency (Hz)		

energy required to melt the ice on the evaporator and the subsequent removal of energy from the evaporator that did not result in ice melting.

A new technique for defrosting refrigeration coils and fin equipment using an applied high voltage AC electric field is presented in this study. The technique, known as the dielectric barrier discharge method (DBD), or corona ice melting technique, involves generating localized heating within an evaporator coil by passing a high voltage, alternating current through insulated electrodes. The discharge generated between the electrodes and the frost formed on the grounded fins melt the frost locally, thus clearing the gap needed for air to flow through the coil. This technique can provide reduced pressure drop in refrigeration equipment and higher defrosting intervals on the evaporators.

2. Background

Electric discharges operated at atmospheric pressure and formed in gaps where at least one electrode is covered by a dielectric barrier are often called dielectric barrier discharges. The dielectric barrier discharge represents the most important non-equilibrium discharge that can be conveniently operated at atmospheric pressure or above. It combines the large volume excitation of the glow discharge with the high pressure of the corona discharge.

A typical configuration for generating dielectric barrier discharges is presented in Fig. 1. The configuration consists of two metallic electrodes, a dielectric layer and an air discharge gap. The air usually flows through the gap formed by the ground potential metal electrode and the dielectric layer, which is in contact with the high voltage electrode.

If the voltage applied to the gas/dielectric combination is V, then the electric fields in the gas gap and dielectric layer E_g and E_d are $E_g = V/k_g$ and $E_d = V/k_d$ respectively, where

$$k_g = \left(d_g + d_d/\varepsilon\right) \quad (1)$$

$$k_d = \left(d_d + \varepsilon \cdot d_g\right) \quad (2)$$

This analysis is valid provided there is no electrical discharge activity in the gas gap. If the applied voltage is increased such that the electric field in the gas gap E_g achieves the breakdown field E_i (~3 kV/mm for air or oxygen), electrical discharges will occur in the gas. These are referred to as 'barrier' discharges [1–3] and each discharge has a channel diameter of 200–500 μm and involves total charge of around 10^{-10} C. These discharges deposit electric charge onto the surface of the dielectric layer, which is of the same polarity as that of the electrode on the other side of the gas gap. Thus, if the voltage in Fig. 1 is positive, when discharging commences, positive charge will be deposited onto the surface of the dielectric contact with the gas. The mobility of charge on most dielectric surfaces is low, and thus the charge may be considered trapped and totally immobile. The charge sets up an electric field, which opposes the field in the gas gap, and discharging in the gas gap at any position will continue until such time as the gas gap

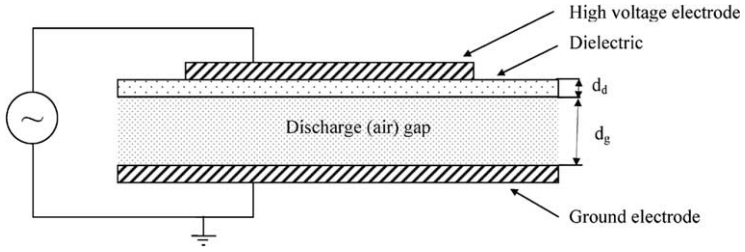

Fig. 1. Typical dielectric barrier discharge configuration.

field at that position has been reduced again to just below the breakdown value. Complete cessation of discharging will occur when the entire dielectric surface is covered with the required density of the charge. If the charge density on the dielectric surface is ρ (C/m^2), then the resultant electric fields in the gas gap and dielectric due to this accumulation of charge are ρ/ε_0 and $\rho/\varepsilon\varepsilon_0$ respectively. The gas gap field, as explained above, opposes the applied field, giving a resultant gas gap field

$$E_g = \left(V/k_g - \rho/\varepsilon_0\right) \tag{3}$$

Therefore the criteria for discharge extinction are

$$E_i = \left(V/k_g - \rho/\varepsilon_0\right) \tag{4}$$

and

$$\rho = \varepsilon_0\left(V/k_g - E_i\right) \tag{5}$$

The electric field in the gas gap is limited to the breakdown field, and discharging will cease when the voltage ceases to increase (i.e. at voltage peak). When the applied voltage then starts to decrease, the charge on the dielectric surface produced by the earlier discharges persists, and the field in the gas gap is reduced at all stages by this constant field, which can be derived as

$$E = \left(V_{max}/k_g - E_i\right) \tag{6}$$

Thus, the field in the gas gap for any instantaneous voltage V will be given by:

$$E_g = V/k_g - \left(V_{max}/k_g - E_i\right) \tag{7}$$

This equation shows that the field in the gas gap can actually become negative before voltage zero and, in fact, depending upon the relative magnitudes of V_{max}/k_g and E_i, can even achieve the breakdown field, heralding the onset of discharges in the opposite direction, before voltage zero. When discharging commences in the opposite direction, the charge on the dielectric surface is rapidly neutralized and replaced with charge of the opposite sign, and the process described above is repeated (see Fig. 2).

Fig. 2 demonstrates the dielectric barrier discharge behavior when a sinusoidal voltage of sufficient amplitude is applied. In this case, a large number of micro-discharges randomly distributed in space and time is induced. At the maximum and minimum applied voltage the displacement current ($dV/dt = 0$) and the micro-discharge activity stops, only to start again when the breakdown field is reached in the gap during the next half-wave. Thus the dielectric serves two functions. It limits the amount of charge and energy that goes into an individual micro-discharge and it distributes the micro-discharges over the entire electrode area. Although the current flows in a large number of individual micro-discharges, the overall electrical behavior of the discharge can be described quite adequately by average

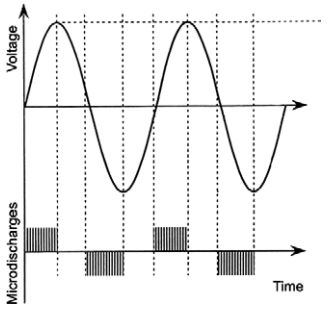

Fig. 2. Schematic diagram of micro-discharge bursts during applied sinusoidal voltage.

quantities. If we denote the discharge voltage V_{DIS} as the average voltage across the discharge gap during the active phases of the discharge, then the power (P) can be expressed as follows:

$$P = \frac{1}{T}\int_0^T VI\,dt = \frac{V_{DIS}}{\Delta T}\int I\,dt \tag{8}$$

The products of such discharges are usually heat and ozone generation. Both of these products can be used or removed in a controlled manner according to the requirements of the target application.

3. Experimental setup

The primary test chamber in which experiments were carried out was a commercial freezer manufactured by a leading supplier of supermarket freezer. A picture of the system and the high voltage equipment used is presented in Fig. 3.

A small evaporator (test section/coil) was mounted inside this test chamber to quantify the effect of the dielectric barrier discharge on frost melting. Two refrigeration loops were used in this setup. The first loop maintained the primary test chamber air temperature within the desired limits. The second loop was used to

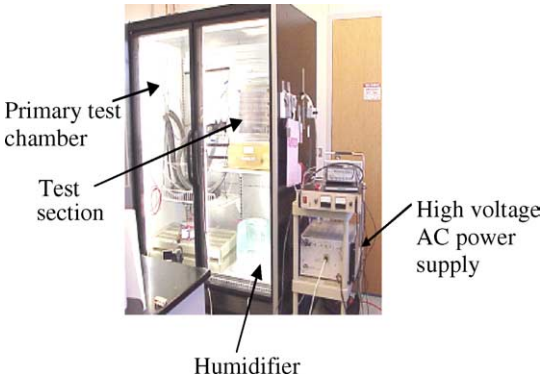

Fig. 3. Photograph of the freezer test chamber.

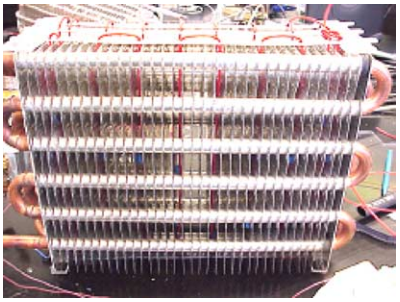

Fig. 4. Photograph of the test evaporator with wire electrodes.

Table 1
Accuracy of the instrumentation

Device	Accuracy of reading
Humidity	±2% (Range: 0–100% RH)
AC high voltage amplifier	0.1% of full scale Less than 30 mV rms output noise
Digital oscilloscope	Sample rates up to 5 GS/s 100 MHz bandwidth

maintained the test evaporator temperature within desired limits. The dimensions of the test evaporator were 0.35 m × 0.12 m × 0.235 m. The evaporator had 34 fins spaced 8 mm apart. The electrode used in these experiments was an insulated wire electrode, which was mounted between the fins of the evaporator as shown in Fig. 4. An ultrasonic humidifier was placed in the test chamber (see Fig. 3) to maintain the humidity levels within predefined limits. The AC high voltage/high frequency power supply consisted of a function generator, a high voltage amplifier, and a digital oscilloscope. The function generator was used to provide a low output voltage (maximum of 10 V) and the shape of the desired wave (i.e., a sine wave). The output of the function generator was then used as the input of the high voltage amplifier, which, in turn, amplified the signal by a maximum of 2000 times. A digital oscilloscope was used to monitor the amplitude, frequency and the shape of the wave of both the voltage and the current at the output of the power supply. The accuracy of the instrumentation used is presented in Table 1.

4. Results and discussion

The preliminary experiments in this study were conducted using single-fin model structures having 100 mm length and 12 mm and 8 mm fin gaps. The thickness of the fins was 1.2 mm. The results obtained with the model fins will be presented first, followed by the results for the prototype test evaporator (shown in Fig. 4).

4.1. Frost melting in model fin geometry

When AC voltages of 7–12 kV with frequencies ranging 700–3000 Hz were applied to wire electrodes placed in the gap between two fins on which frost was accumulated, intense melting of frost occurred. The fins were cleared of frost within 2–3 min, removing the thermally insulating frost layer and allowing air to flow again between the fins.

Fig. 5 presents the effect of the DBD heating technique on the melting of frost grown for 2 h with a fin gap of 8 mm. The time needed to completely clear the fins' surface was about two minutes when the applied voltage and frequency were $V = 12$ kV and $f = 700$ Hz.

The electrodes used in these experiments were Teflon-based insulated wires. The dimensions of the wires were $D_i = 0.89$ mm and $D_o = 1.82$ mm. The melting of the frost was localized because of the distribution of the energy in the dielectric barrier discharge (see Fig. 6). As can be seen in Fig. 5, the frost melted on the fins on each side of the electrode, but the frost on the other side of these fins did not melt.

This localized melting indicates that the discharge was melting the frost layer by layer. Nozaki et al. [4,5] estimated from their DBD experiments using one insulated electrode (see Fig. 6a) that 80% of the input power was converted into the heating of the electrodes. They estimated 60% of the total power heated the dielectric electrode, and 20% heated the metallic electrode. Since the frost/ice formed on the cold fins has dielectric properties, the shape and energy distribution of the micro discharge filaments is believed to be better represented by Fig. 6b, even though the grounded fin is uninsulated metal.

Temperature measurements on the fins in dry conditions indicated a 20–30 °C increase in fin temperature after several minutes. A uniform, steady, blue light forming around the wire, associated with thin filaments, was observed as the voltage reached our operating conditions of voltage and frequency (see Fig. 7).

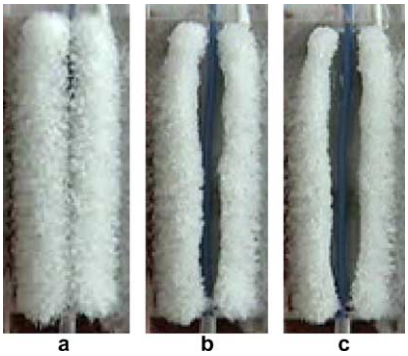

Fig. 5. DBD frost melting on fins: (a) frost before DBD; (b) DBD applied for 1 min and (c) DBD applied for 2 min.

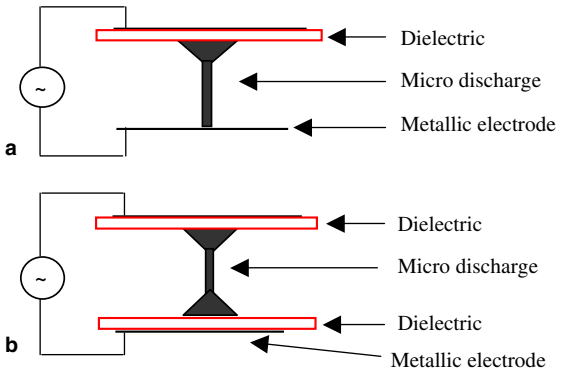

Fig. 6. Schematic of micro-discharge filaments (not to scale): (a) single dielectric layer and (b) double dielectric layer.

The localized nature of this discharge makes this technique very attractive for refrigeration systems, since the air temperature in the gap does not increase substantially. Also, the degree of frost removal is controllable, so the air passages within the evaporator can be cleared without removing all the frost, thereby minimizing the heating of the evaporator.

4.2. Frost melting in the test evaporator

As shown in Fig. 8, fast frost melting was obtained using an AC voltage of 12 kV at frequencies from 700 Hz to 5000 Hz. As the frost started to melt layer by layer, the gap between fins was cleared for unobstructed air flow. Complete melting was obtained after 2–3 min.

As we attached electrodes to a larger area of the evaporator, the current limit ($I_{max} = 10$ mA) of the power supply was exceeded, so the required voltage to generate the corona could not be generated. For the size of our test evaporator, our power supply could generate enough power to defrost two entire fins. These two fins could be defrosted within about 3 min, with a power consumption ranging 35–45 W.

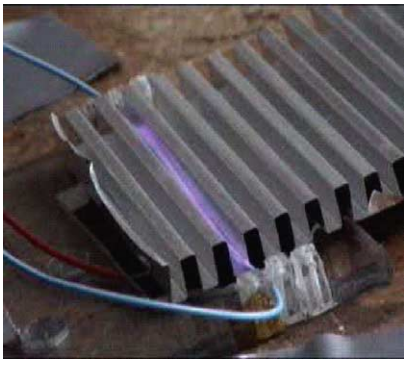

Fig. 7. Photograph of corona around insulated electrode between fins.

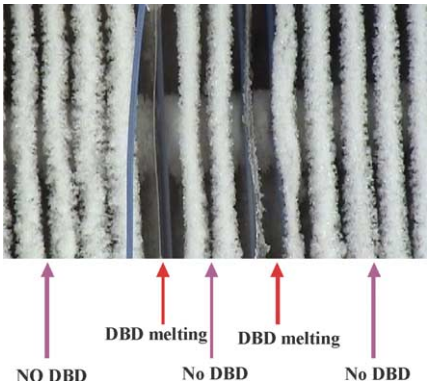

Fig. 8. Defrosting using dielectric barrier discharge.

The defrosting of the entire 32 fins of our evaporator could be accomplished by wiring the evaporator in sections, and defrosting each section in turn, as shown in Fig. 9. We estimated that the entire test evaporator could defrost in about 50 min with a total energy consumption of 130 kJ.

Besides saving energy, this defrosting technique would minimize the food warming that occurs during a defrost cycle of a freezer. In this defrosting technique, only a small portion of the evaporator could be defrosted at any one time, so the average temperature of the entire evaporator would be largely unaffected. Thus, the temperature of the food in the refrigerator would not increase, which would improve food quality. The generation of ozone could also be beneficial as an antibacterial treatment, as its concentration can be controlled using ozone filters.

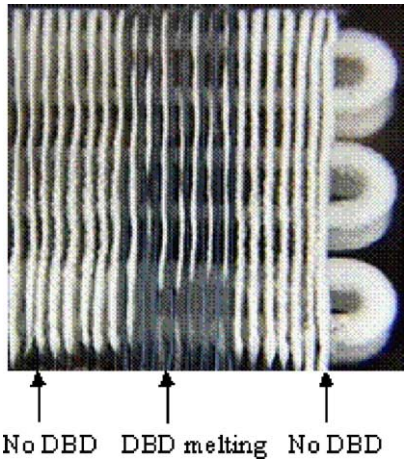

Fig. 9. Defrosting using DBD in each section of the evaporator.

5. Comments on the electrode dielectric properties

As explained above, DBD or corona heating is the mechanism responsible for the frost melting via electrodes to which high voltage AC power (7–2 kV and $f = 700$–3000 Hz) is applied. To withstand potential sparking and the harsh environment (i.e. corona discharge), the dielectric electrodes must possess the following properties:

- High breakdown voltage.
- High dielectric strength.
- Low dissipation factors (to minimize power consumption).
- Low dielectric absorption (to minimize heating of the insulation).

A series of electrodes with insulation of various types and thicknesses were tested to determine their effect on corona melting. Experiments were conducted on a small section of stand-alone fin stock (outside of the refrigeration system). The wires were evaluated by monitoring the fin temperature as a function of time. Sample fin temperature measurements as a function of power consumption are shown in Figs. 10 and 11.

As shown by Fig. 10, the temperature rise of the fin was faster at a higher frequency applied voltage even at the same input power, as expected.

A comparison of two electrodes with different insulating materials is shown in Fig. 11. The irradiated polyolefin insulation (XLPE) heated the fin to a higher temperature at a given power level than the FEP insulation. Most of the insulation tested generated less heating of the fin than these two types. It was also observed that the fin temperatures for the polyolefin insulation wire mounted on the fin were higher for the range of tested

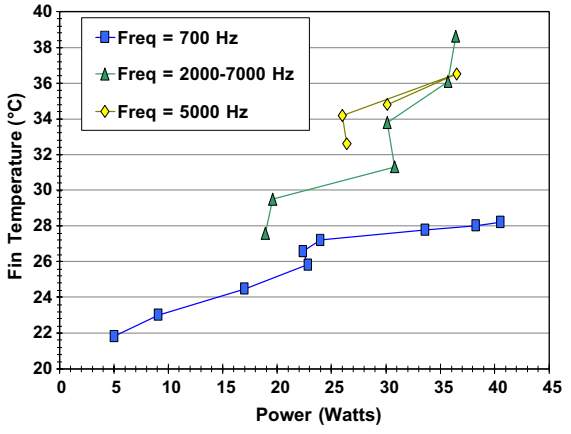

Fig. 10. Fin temperature as a function of power for an electrode with 0.4 mm FEP insulation.

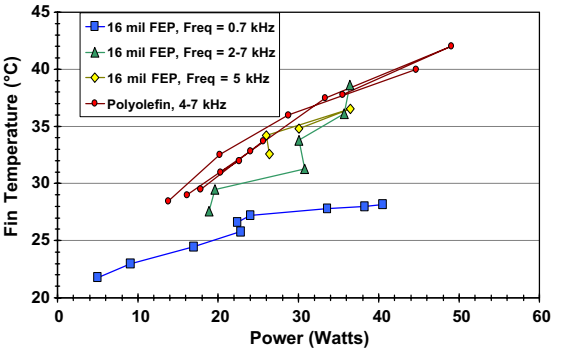

Fig. 11. Fin temperature as a function of power consumption for 0.4 mm FEP and 0.38 mm XLPE insulations.

frequencies, and for the same power levels compared to those recorded when type 316 stainless steel wire was used. This is graphically shown in Fig. 11.

Another difference among the types of insulation tested was the length of time over which a corona could be generated before the onset of sparking due to a breakdown of the electrode's insulation. The lifetime of some tested insulation was as short as 25 min while the XLPE and FEP insulations were still operational after 24 h of continuous testing. This difference emphasizes the importance of the electrical properties required by the electrode as presented above.

6. Frost melting via DBD versus electrical heating

We compared the defrost power consumption levels required for the DBD/corona melting and the electrical melting techniques. For DBD melting, the test evaporator would require 36.5 m (120 ft) of electrodes length to cover its surface area. DBD defrosting requires about 7 W per foot of electrode for 3–4 min to completely defrost the fins. Thus, the energy required for the DBD process would be about 0.6 MJ/m (i.e. 50–60 W h per foot).

The electrical defrosting technique required about 300 W of power for 15–20 min to defrost the evaporator. Thus the energy requirements for electrical defrost was about 1.0 MJ/m (about 75–100 W h per foot). Therefore, the DBD melting technique would save about 0.4 MJ per meter of evaporator during each defrosting cycle.

7. Conclusions

The innovative dielectric barrier discharge (DBD) method of defrosting was discussed in this paper. The DBD method requires the use of AC voltages in the range of 7–12 kV at a frequency of 700–5000 Hz. Experiments were also performed where defrosting was

achieved at lower frequencies (i.e. 50 Hz). However, additional tests are needed to quantify the more accurate range of voltage and frequency requirements for optimized defrosting. Defrosting an evaporator in sections using this technique will minimize both the power load required and the defrosting time, thus substantially reducing the defrost power consumption, while also avoiding frequent thermal cycling of the food products for quality preservation. Our ongoing experiments involve developing techniques to evaluate critical properties of the insulation on the electrodes, thus improve life and reliability of the electrodes.

Acknowledgements

This work was carried out under a USDA SBIR Phase II contract (#2001-33610-11099) and with additional support of the Hussmann Corporation. The authors are grateful for the support of these sponsors.

References

[1] B. Eliasson et al., Modeling and applications of silent discharge plasmas, IEEE Trans. Plasma Sci. 19 (2) (1991).
[2] J.S. Chang, A.J. Kelly, J.M. Crowley, Handbook of Electrostatic Processes, Marcel Dekker, Inc., 1995, ISBN 0-8247-9254-8.
[3] J. Tepper, P. Li, M. Lindmayer, Effects of interface between dielectric barrier and electrode on homogeneous barrier discharges at atmospheric pressure, in: XIV International Conference on Gas Discharges and their Application, Liverpool, 01–06 September, 2002.
[4] T. Nozaki, Y. Miyazaki, Y. Uno, K. Okazaki, Energy distribution and heat transfer in atmospheric pressure non-equilibrium plasmas, in: 15th Symposium on Plasma Chemistry, Orleans, France, vol. 4, July 2001, pp. 1591–1596.
[5] T. Nozaki, Y. Miyazaki, Y. Uno, K. Okazaki, Energy distribution and heat transfer in atmospheric pressure non-equilibrium plasmas, J. Phys. D: Appl. Phys. (34) (2001) 3383–3390.